# Raman resonance window of single-wall carbon nanotubes

J. S. Park,[1,*] Y. Oyama,[1] R. Saito,[1,†] W. Izumida,[1] J. Jiang,[1] K. Sato,[1] C. Fantini,[2] A. Jorio,[2] G. Dresselhaus,[3] and M. S. Dresselhaus[4,5]

[1]*Department of Physics, Tohoku University and CREST, Sendai, 980-8578, Japan*
[2]*Departamento de Física, Universidade Federal de Minas Gerais, Belo Horizonte-MG, 30123-970, Brazil*
[3]*Francis Bitter Magnet Laboratory, Massachusetts Institute of Technology, Cambridge, Massachusetts 02139-4307, USA*
[4]*Department of Electrical Engineering and Computer Science, Massachusetts Institute of Technology,*
*Cambridge, Massachussetts 02139-4307, USA*
[5]*Department of Physics, Massachusetts Institute of Technology, Cambridge, Massachusetts 02139-4307, USA*

The spectral width, or $\gamma$ value, of the Raman excitation profile for single-wall carbon nanotubes is calculated by evaluating the lifetime of the carriers. The calculated results for the $\gamma$ values are compared with the experimental spectral width of the Raman excitation profile. The $\gamma$ values evaluated by the electron-phonon interaction show a strong chirality and diameter dependence which is crucial for obtaining the peak intensities of the resonance Raman spectra. Moreover, for metallic carbon nanotubes, we expect an additional contribution to the calculated $\gamma$ values by comparing them with the experimental results. In particular, we expect that the plasmon excitation in metallic carbon nanotubes may also contribute to the spectral linewidth $\gamma$.

## I. INTRODUCTION

Resonance Raman spectroscopy of single-wall carbon nanotubes (SWNTs) has been widely used for evaluating the sample quality[1] and population[2] of individual $(n,m)$ SWNTs in actual samples. In the analysis of Raman spectra, not only the resonance energies for a given $(n,m)$ SWNT, but also the Raman intensities relative to the intensity of other $(n,m)$ SWNTs or of other phonon modes are important for evaluating the populations of SWNTs in the mixed sample. In previous papers, by using an extended tight binding calculation of the electronic[3] and phonon[4] structures, we showed the presence of a strong $(n,m)$ chirality and diameter dependence of the radial breathing modes (RBM) and the G-band Raman intensity[4,5] and of the photoluminescence (PL) intensity.[6] The calculated results have been directly compared with (1) experimental PL intensity measurements on samples prepared at different synthesis temperatures,[6] (2) experimental Raman/PL intensity ratio measurements,[7] and (3) direct transmission electron microscope measurements of the diameter distribution.[8] The agreement between theory and experiment is satisfactory except for some exceptions for small diameter SWNTs.

In the resonance Raman intensity formula [see Eq. (1)], we have two energy difference denominators $(E_L - E_\mu - i\gamma)$ and $(E_L - E_\mu - E_{ph} - i\gamma)$ coming from time-dependent perturbation theory. Very close to resonance, we have $E_L = E_\mu$ or $E_L = E_\mu + E_{ph}$, and we find that the large resonance enhancement of the Raman intensity is very sensitive to the $\gamma$ value. Here $E_L$, $E_\mu$, and $E_{ph}$ are, respectively, the laser excitation energy, the excitonic transition energy, and the phonon energy. Experimentally we can observe this $\gamma$ value as the spectral width of Raman spectra as a function of excitation laser energy[9] (Raman excitation profile, REP), and we see both a diameter and chiral angle dependence of the $\gamma$ values. Moreover, it seems that the $\gamma$ value for metallic SWNTs ($M$-SWNTs) is larger than that for semiconducting SWNTs

($S$-SWNTs).[9] However, in previous intensity calculations,[2] we used a constant value 0.06 eV for the $\gamma$ values for all SWNTs. This might be the reason why we do not get good agreement between the calculated and experimental values for smaller diameter SWNTs.[7] In order to get more reliable calculated intensity values, we calculate the $\gamma$ value as a function of $(n,m)$ in the present paper.

For a resonance system, the resonance width is related to the energy dissipation, and in quantum mechanics, the width is related by the uncertainty relation to the lifetime of the carriers. The dominant origin of the lifetime of the carriers in the Raman spectra is inelastic scattering by the emitting and absorbing phonons. In this paper, we calculate the carrier lifetime[10] by considering electron-phonon matrix elements[4,5] and the Fermi golden rule. We further consider the electron-plasmon coupling for possible contributions to shortening the lifetime (broadening the $\gamma$ value) by plasmon excitations especially for $M$-SWNTs. Recent experiments by Akima *et al.*, show that a possible plasmon excitation at lower energy levels occurs because of the finite length of SWNTs (Ref. 11) and thus we conclude that plasmons should be relevant to the present paper.

In Sec. II, measurements of $\gamma$ values are presented. In Sec. III, we show how to calculate the resonance Raman profile and we show calculated $\gamma$ values for both semiconducting and metallic carbon nanotubes. We also directly compare the calculated $\gamma$ values with experimental values. In Sec. IV, a summary of this work is given.

## II. $\gamma$ VALUE MEASUREMENTS

The experimental resonance window was measured for various samples at room temperature and at ambient pressure, using a DILOR *XY* triple-monochromator spectrometer in a backscattering configuration, equipped with a liquid $N_2$ cooled charge coupled device. The samples were excited by a tunable laser system composed of a Ti:sapphire laser, a dye
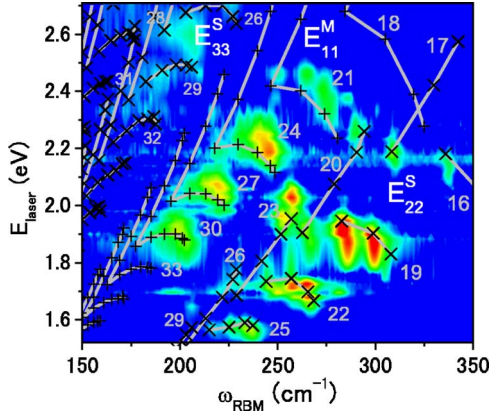
FIG. 1. (Color online) The experimental 2D resonance Raman plot (intensity increases from blue to red) compared with resonance points calculated by the extended tight binding method presented in a Kataura plot (+ for metallic and × for semiconducting nanotubes). SDS-wrapped HiPCO carbon nanotubes in solution were used in the experiment. We can see that, for metallic nanotubes, the experimental peaks are related only to the lower transition energy compared to the extended Kataura plot. The numbers denote values of $2n+m$.

laser, and a Ar-Kr ion laser. This system provides a quasi-continuous variation of excitation energies in the range 1.52 to 2.71 eV.[9]

In Fig. 1, a RBM Raman intensity map is plotted by color as a function of RBM frequency ($\omega_{\text{RBM}}$) and excitation energy. The symbols + and × denote the resonant transition energies calculated by the extended tight binding method for $M$-SWNTs and $S$-SWNTs, respectively.[3] The calculated and experimental points, both show family patterns with the same $2n+m$ values in Fig. 1. Along a vertical line, an experimental REP for individual RBM features was obtained for the different $(n,m)$ SWNTs present in the sample. From these measurements, we can thus obtain the experimental linewidth ($\gamma_{\text{EX}}$) values of the resonance Raman profiles for individual $(n,m)$ nanotubes. Experimental results reveal that the $\gamma_{\text{EX}}$ value, representing the lifetime broadening of the excitonic transition of an individual $(n,m)$ nanotube, is different for each $(n,m)$ nanotube in a given sample.

We show in Fig. 2 the REPs of the RBM at 310 cm$^{-1}$ observed for (6,5) nanotubes in (a) CoMoCAT (Ref. 12) and (b) HiPCO (Ref. 13) samples. Solid circles and open squares denote SDS-wrapped SWNTs in solution and SWNTs within bundles, respectively. Solid and dashed lines represent the fit of the REPs to the following equation:

$$I(E_L) \propto \int \left| \frac{M_\mu^{\text{op}} M^{e\text{-ph}} M_\mu^{\text{op}}}{[E_L - E_\mu(k) - i\gamma][E_L - E_\mu(k) - E_{\text{ph}} - i\gamma]} \right|^2 dk,$$

(1)

where the matrix elements for optical absorption $M^{\text{op}}$, electron-phonon coupling $M^{e\text{-ph}}$, and optical emission $M^{\text{op}}$ are taken as constants for the fitting. In the following section, we calculate the matrix elements by the extended tight binding method.[4] The $\gamma_{\text{EX}}$ value is determined by fitting the parameter $\gamma$ of Eq. (1) to the experimental points. For the Co-
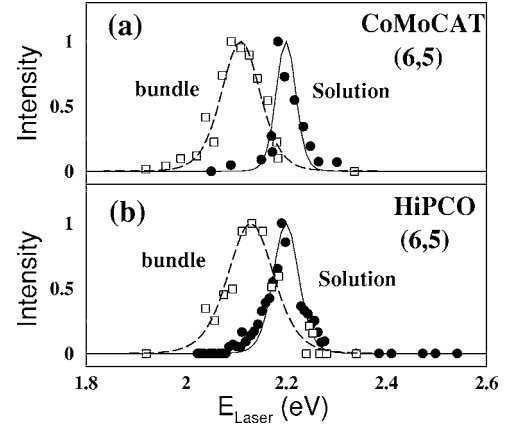


FIG. 2. The RBM intensity at 310 cm$^{-1}$ is plotted as a function $E_{\text{Laser}}$ for bundle SWNTs and for SDS wrapped (6,5) SWNTs in solution for (a) CoMoCAT and (b) HiPCO samples.

MoCAT nanotubes in solution, the REPs show a smaller linewidth than those for HiPCO nanotubes in solution. The $\gamma_{\text{EX}}$ values of (6,5) nanotubes for HiPCO and CoMoCAT samples in solution are 63 meV and 40 meV, respectively. Moreover, the linewidth for SWNTs in solution is smaller than that for bundles, which means that there are more relaxation paths for excited carriers in bundles than for isolated SWNTs. For example, the tube-tube interaction may make the carrier relaxation to other SWNTs possible. When we compare the REPs for HiPCO and CoMoCAT SWNTs in solution, we can see that there are only very minor differences in the optical transition energies due to environmental effects. It should be mentioned that the $\gamma_{\text{EX}}$ for CoMoCAT SWNTs is not always smaller for all $(n,m)$ tubes than the $\gamma_{\text{EX}}$ for HiPCO SWNTs. Thus the 23 meV difference should be considered as a sample- and $(n,m)$-dependent deviation.

### III. RELAXATION TIME CALCULATION

Here we calculate the transition rate for an excited electron scattered to the other electronic states by emitting or absorbing a phonon. The inverse of this transition rate is called the relaxation time $\tau$,[6,14] which is inversely proportional to the resonance window, i.e., to the $\gamma$ value, and the $\gamma$ satisfies the uncertainty principle,

$$\gamma = \frac{\hbar}{\tau}.$$

(2)

The transition rate for the scattering of an excited electron from an initial state $\mathbf{k}$ to all possible final states $\mathbf{k}'$ by the $\nu$-th phonon mode per unit time can be obtained by the Fermi golden rule,[6]

$$\frac{1}{\tau_\nu} = W_{\mathbf{k}}^\nu = \frac{S}{8\pi M d_t} \sum_{\mu',k'} \frac{|D_\nu(\mathbf{k},\mathbf{k}')|^2}{\omega_\nu(\mathbf{k}'-\mathbf{k})} \left( \frac{dE(\mu',k')}{dk'} \right)^{-1}$$

$$\times \left( \frac{\delta[\omega(\mathbf{k}') - \omega(\mathbf{k}) - \omega_\nu(\mathbf{k}'-\mathbf{k})]}{e^{\beta\hbar\omega_\nu(\mathbf{k}'-\mathbf{k})} - 1} \right.$$

$$\left. + \frac{\delta[\omega(\mathbf{k}') - \omega(\mathbf{k}) + \omega_\nu(\mathbf{k}'-\mathbf{k})]}{1 - e^{-\beta\hbar\omega_\nu(\mathbf{k}'-\mathbf{k})}} \right),$$

(3)

where $S$, $M$, $d_t$, $\beta$, and $\mu'$ denote the area of the 2D graphite unit cell, the mass of a carbon atom, the diameter of a SWNT, $1/k_BT$ ($k_B$, the Boltzmann constant), and the cutting line indices of the final state, respectively. $D_\nu(\mathbf{k},\mathbf{k}')$ is a matrix for scattering an electron from $\mathbf{k}$ to $\mathbf{k}'$ by the $\nu$-th phonon mode. The relaxation process is restricted to satisfying energy-momentum conservation. The two terms in large parentheses in Eq. (3), respectively, represent the absorption and emission processes of the $\nu$-th phonon mode with energy $\hbar\omega_\nu(\mathbf{k}'-\mathbf{k})$.

### A. Semiconducting SWNTs

For each phonon mode and for each energy band, we have (1) forward and backward scattering, and (2) intravalley and intervalley scattering. Since we have six branches of phonon modes, we expect 24$\mathbf{k}'$ states for each $\mathbf{k}$ of each energy subband.[4] As an initial state, we consider only an excited electron in the bottom of the second conduction band $c_2$ which relaxes to the first conduction band $c_1$, because only a few photoexcited electrons contribute to the scattering process, and the relaxation rate by a phonon is faster (0.1 ps) than the photon emission process (0.1 ns).[15] The intravalley transition is mostly associated with four types of phonons, namely, the iLO [$\sim$0.025 ps for the (6,4) tube], iTO($\sim$6.59 ps), oTO ($\sim$0.036 ps), and RBM ($\sim$0.1 ps) phonons, because of the flatness of the phonon dispersion curves near the $\Gamma$ point. In these modes, the coupling with the iLO mode is the strongest due to the longitudinal vibration of the C-C bond. The intervalley transition corresponds to phonons near the $K$ points, including all six phonon modes. Therefore, all these phonon modes have a large phonon DOS in the vicinity of the $K$ point. Among the six phonon modes, the iLO and iLA modes give the strongest electron-phonon coupling and thus contribute strongly to relaxation processes compared with other modes.

It is important to consider the energy difference between the two conduction bands in the phonon scattering process, because the energy difference gives a restriction on the scattering that can occur between the electron and the phonon mode. In Fig. 3(a), we plot schematically the energy difference between the conduction bands, $c_2$ and $c_1$, as a function of tube diameter for types I and II $S$-SWNTs: type I [$(2n+m)\bmod 3=1$], and type II [$(2n+m)\bmod 3=2$]. As seen in Fig. 3(a), the energy difference $\Delta E_{c_2-c_1}$ shows family patterns for both types I and II tubes, and we see that $\Delta E_{c_2-c_1}$ (type I) $<\Delta E_{c_2-c_1}$ (type II). Two dashed lines in Fig. 3(a) indicate the iLO phonon energy at the $K$ (0.16 eV) and $\Gamma$ (0.20 eV) points in the Brillouin zone, respectively. The $(n,m)$ nanotubes (8,0), (7,2), (9,1), and (11,0) which have $\Delta E_{c_2-c_1}$ less than 0.16 eV cannot emit iLO and iTO phonons by scattering because of energy-momentum conservation requirements, and thus a relatively long lifetime (small $\gamma$ value) is obtained for these tubes [see Fig. 4(a)]. It should be mentioned that $\Delta E_{c_2-c_1}$ for the (8,0) nanotube is negative by the definition of the $c_1$ and $c_2$ energy bands, in which the $c_1$ ($c_2$) band is defined not by the energy band minimum, but by the cutting line closest (next closest) to the $K$ point. The
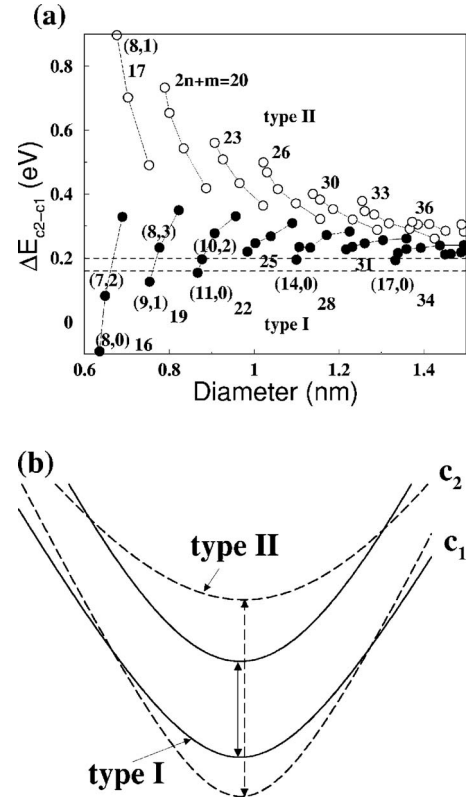


FIG. 3. (a) Energy differences at the energy extrema between the $c_1$ and $c_2$ conduction bands. Two dashed lines indicate the iLO phonon at the $K$(0.16 eV) and $\Gamma$(0.20 eV) points, respectively. Filled and open circles denote type I and type II nanotubes, respectively. (b) Energy dispersion in the conduction bands $c_1$ and $c_2$. Energy bands for type I and type II $S$-SWNTs are plotted by solid lines and dashed lines, respectively. For comparing type I with type II conduction bands, we overlap these conduction bands for the two types of tubes at the $\mathbf{k}$ axis.

nanotubes lying on the two dashed lines, such as (10,2), (8,3), and (17,0), are remarkably resonant with the iLO phonon at the $\Gamma$ point. The "resonance" or "restriction" effects related to phonon scattering appear only for type I nanotubes. The reason for the different $\Delta E_{c_2-c_1}$ values between type I and II nanotubes is due to the energy dispersion in the conduction band, as shown in Fig. 3(b). While the two conduction bands for type I nanotubes (solid lines) are parallel to each other, the two curvatures for type II nanotubes (dashed lines) are different from each other, i.e., the curvature for band $c_1$ is larger than the curvature for band $c_2$. Accordingly, the DOS of the final state, $(dE/dk)^{-1}$, for an electron to relax from the bottom point of band $c_2$ to band $c_1$ depends on whether they are type I or II tubes, since DOS(type I)$>$DOS(type II).

In Fig. 4(a), we plot $\gamma$ values for the relaxation time for $S$-SWNTs, when an excited electron in the bottom of $c_2$ relaxes to $c_1$. The distribution of $\gamma$ values for $(n,m)$ $S$-SWNTs in Fig. 4(a) is derived by substituting for the relaxation time using Eq. (2). As seen in Fig. 4(a), the $\gamma$ values are inversely proportional to the diameter of $S$-SWNTs, and type I SWNTs give larger $\gamma$ values than type II SWNTs for the large diameter range ($>$1.0 nm). The $S$-SWNTs near armchair tubes

**(a)**



**(b)**
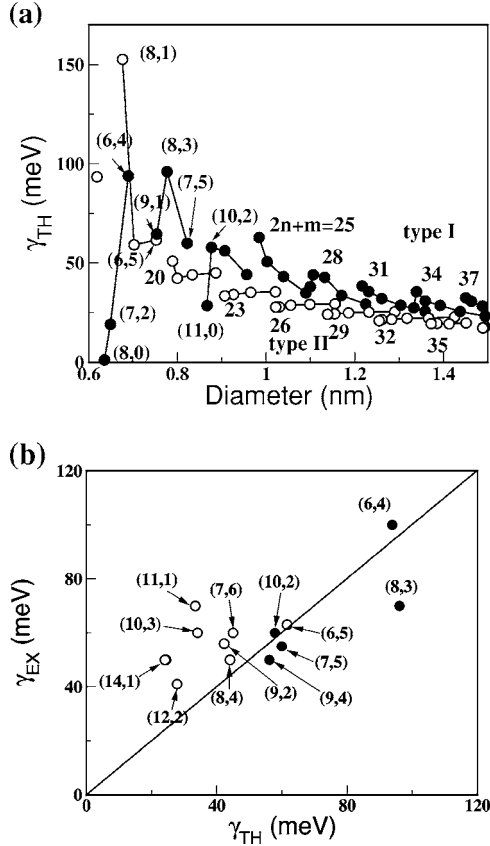


FIG. 4. (a) Calculated $\gamma$ values for $S$-SWNTs for $0.6 < d_t < 1.5$ nm. Filled and open circles indicate type I and type II $S$-SWNTs, respectively. The $\gamma$ value for an (8,0) nanotube is near to 0 meV, because of the absence of iLO phonon scattering. (b) Comparison of the calculated $\gamma$ value ($\gamma_{TH}$) with the experimental $\gamma$ value ($\gamma_{EX}$). Experimental $\gamma$ values were measured by plotting the RBM intensity for HiPCO-SWNTs in SDS solution at 300 K with a change of the laser energy. Filled and open circles indicate type I and type II $S$-SWNTs, respectively.

($\theta \sim 30°$) give relatively similar $\gamma$ values between type I and II SWNTs, while $S$-SWNTs near zigzag tubes ($\theta \sim 0°$) gives a relatively large difference of $\gamma$ values between type I and II SWNTs. In the small diameter range ($< 0.9$ nm), some $S$-SWNTs of type I near ($\theta \sim 0°$), such as (8,0), (7,2), (9,1), and (11,0), have small $\gamma$ values as compared to type II SWNTs. In the case of the (9,1) nanotube, however, because of the resonance with the "iTA or iLA mode" at the $K$ point, the $\gamma$ value becomes relatively large. These $S$-SWNTs have $\Delta E_{c_2 - c_1}$ values smaller than 0.16 eV, which is the lower limit for exciting the iLO phonon mode. The (8,1) type II nanotube has a large $\gamma_{TH}$ value contrary to other type II nanotubes, because its conduction bands $c_2$, $c_3$, and $c_4$ occur within a small energy region, and thus, we can easily find a scattering process to their many energy subbands. In Fig. 4(b), the $\gamma_{TH}$ values calculated by the above process are compared with the experimental resonance width $\gamma_{EX}$ obtained from the RBM Raman spectral intensity profile for the HiPCO sample. When we compare the calculated $\gamma_{TH}$ value with $\gamma_{EX}$, the agreement is satisfactory. For (6,4), (6,5), and (7,5) nanotubes, the calculated $\gamma_{TH}$ and experimental $\gamma_{EX}$

values ($\gamma_{TH}$, $\gamma_{EX}$) are (94, 100 meV), (62, 63 meV), and (60, 55 meV), respectively. Compared with type I tubes, $\gamma_{EX}$ for type II tubes is always larger than $\gamma_{TH}$, showing that there are additional relaxation paths yet to be identified.

**B. Metallic SWNTs**

Next, we consider electron-phonon scattering in the transition process of $M$-SWNTs. An excited electron in the $c_1$ band scatters to a metallic energy band by interaction with a phonon, satisfying momentum-energy conservation. The $\gamma$ value is obtained by calculating the relaxation time for an electron in the bottom of the $c_1$ band $E_{11}(H)$ [or $E_{11}(L)$] to relax to $E_{11}(L)$ (or to two linear energy bands). We consider the same scattering process as for $S$-SWNTs to calculate the relaxation time of $M$-SWNTs. We should also consider an excited electron to scatter with six phonon modes in the $c_1$ band. For small diameter ($< 0.8$ nm) $M$-SWNTs, the transition rate by RBM($\sim 0.024$ ps) scattering is strongest, while the transition rate by iLO($\sim 0.043$ ps) scattering is small compared with RBM scattering. Because of the curvature effect on, for the electron-phonon matrix element, the RBM phonon mode becomes large.[4] Here the numerical values are for a (7,1) SWNT.

Figure 5 shows $\gamma$ values for $M$-SWNTs. Two types of transitions appear in Fig. 5 because of the DOS splitting due to the trigonal warping effect.[16] One is a transition from $E_{11}(H)$ (solid circles) in $c_1$, and the other is from $E_{11}(L)$ (open circles). Here, $H$ and $L$ denote higher and lower energy for the metallic $E_{11}$ energy band. The $\gamma$ value for $E_{11}(L)$ shows a diameter dependence and no significant chirality dependence, because the DOS of the final state in the two linear energy bands is constant (no chiral angle dependence) in the case of phonon emission. In detail, while the $\gamma$ value for RBM scattering depends on chirality and diameter, that for other phonon modes shows only a diameter dependence. However, the $\gamma$ value for $E_{11}(H)$ shows both a chirality and a diameter dependence. The chirality dependence comes from the scattering processes to the $E_{11}(L)$ band as a final state. Nevertheless, when we calculate the REP by considering the matrix elements, the higher energy REP peak is generally smaller in intensity than the lower energy REP peak because of the small value of the matrix element. Thus, even though the energy separation between $E_{11}(H)$ and $E_{11}(L)$ is sufficiently small compared with the $\gamma$ value, the overall $\gamma$ values are not significantly affected by the $E_{11}(H)$ peak. When we compare the above calculation results with the experiments, the theoretical $\gamma_{TH}$ values are always smaller than the experimental $\gamma_{EX}$, as shown in Fig. 5(b). In the case of the (11,8) nanotube, for example, $\gamma_{TH}$ and $\gamma_{EX}$ are 25 and 140 meV, respectively. This implies that for the case of this $M$-SWNT, additional processes which are different from environmental or defect-related effects, might also be important as well as the electron-phonon interaction.

One possibility for explaining the additional contribution to the relaxation process in $M$-SWNTs is identified with the interaction of an excited electron with the conduction electrons in the two linear energy bands. The one-dimensional correlated electrons in two linear energy bands behave as a

**(a)**



**(b)**
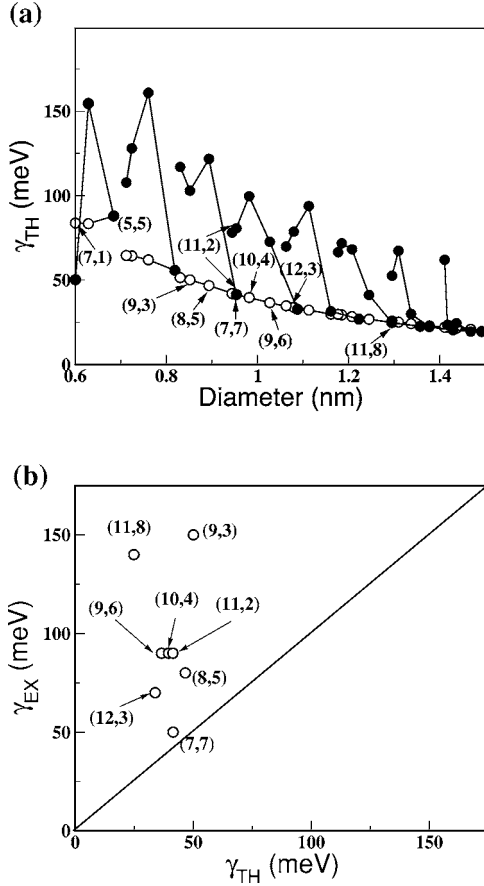


FIG. 5. (a) Calculated $\gamma$ values for $M$-SWNTs in the diameter range, $0.6 < d_t < 1.5$ nm. Filled and open circles indicate $E_{11}(H)$ and $E_{11}(L)$, respectively. (b) Comparison of $\gamma_{TH}$ with experimental $\gamma_{EX}$ values for $M$-SWNTs.

Tomonaga-Luttinger (TL) liquid.[17–19] The collective excitation is an essential excitation, and the collective excitation for a charge carrier is the plasmon. The interaction between the excited electron and the conduction electrons can be written in terms of the electron-plasmon interaction. In analogy to the deformation potential associated with long wavelength phonons,[20] we assume the following interaction between electrons and plasmons:

$$H_{\text{el-pl}} = V_{\text{el-pl}} \int dx \rho_{\text{pl}}(x) \rho_e(x), \tag{4}$$

where $V_{\text{el-pl}}$ is the coupling constant between an electron and a plasmon, $\rho_{\text{pl}}(x)$ is the charge density caused by the plasmon, and $\rho_e(x)$ is the electron density in the conduction band $c_1$, and the $x$ axis is taken along the tube and the axis along the circumferential direction has been integrated out. The Hamiltonian of the plasmon is

$$H_{\text{pl}} = \frac{v_{\text{pl}}}{2} \int dx \left( g_{\text{pl}}[\Pi(x)]^2 + \frac{1}{g_{\text{pl}}}[\partial_x \phi(x)]^2 \right), \tag{5}$$

where $g_{\text{pl}}$ is the interaction parameter of the TL liquid, and $v_{\text{pl}}$ is the velocity of the plasmon. $\Pi(x)$ and $\phi(x)$ play the role of the momentum and displacement field operators, re-

spectively, and they are conjugate variables to each other, i.e., $[\phi(x), \Pi(x')] = i\hbar \delta(x - x')$. The charge density follows the relation $\rho_{\text{pl}}(x) = 2\partial_x \phi(x)/\sqrt{\pi \hbar}$. Using the Hamiltonian in Eq. (5), we can calculate the relaxation time of the excited electron in the same way as for the case of the electron-phonon scattering. After some calculation, we get the following analytical expression for the lifetime of the excited electron at the bottom of the band $c_1$:

$$\frac{1}{\tau} = \frac{8m^*}{\pi \hbar^3} g_{\text{pl}} |V_{\text{el-pl}}|^2 n_{\mathbf{k}_0}. \tag{6}$$

Here $m^*$ is the effective mass of the excited electron in band $c_1$. This term appears because of the electron-plasmon scattering in the band $c_1$. A plasmon with momentum $|\mathbf{k}_0| = 2m^* v_{\text{pl}}/\hbar$ is absorbed in this process, and therefore the Bose-Einstein distribution function $n_{\mathbf{k}_0}$ appears. Even though the precise estimation of $1/\tau$ is difficult because of the uncertain parameters, $g_{\text{pl}}$, and $V_{\text{el-pl}}$, we nevertheless here estimate the numerical value of the lifetime. Let us assume that $V_{\text{el-pl}}$ is on the order of the bandwidth, then $V_{\text{el-pl}} \approx 3$ eV Å. The TL parameter $g_{\text{pl}}$ strongly depends on the system,[20] and would have a value in the range $0.2 < g_{\text{pl}} < 1$, that is, $g_{\text{pl}} \simeq 0.2$ for isolated conditions while $g_{\text{pl}} \simeq 1$ for well-screened (noninteraction) conditions. For the present argument, we now assume $g_{\text{pl}} = 1$. The effective mass depends on the chirality, and most of the $M$-SWNTs have values in the range $0.1 < m^*/m_e < 0.2$, where $m_e$ is the free electron mass. Now we use $m^*/m_e = 0.1$ for the estimation, and then these values give $\gamma \simeq 0.3 n_{\mathbf{k}_0}$ eV. At room temperature, $n_{\mathbf{k}_0}$ is almost zero because the $\mathbf{k}_0$ plasmon has a large energy, $\hbar v_{\text{pl}} k_0 \sim 0.7$ eV. At a glance, there are no plasmon scattering processes at room temperature. However, we must carefully consider the experimental situation; to excite an electron to the band $c_1$ we use an incident laser with an energy in the $1-3$ eV range. It is natural to consider that the incident laser also excites the electrons in the linear energy bands. After relaxation in the linear energy bands, there would be a finite population of electrons at the $\mathbf{k}_0$ plasmon. Even though the quantitative estimation of $n_{\mathbf{k}_0}$ is difficult, numerical estimates of $n_{\mathbf{k}_0}$ might be on the order of 1. We note that the relaxation time in the linear energy bands is about 10 times faster than that in the $c_1$ band.[21,22]

The other scattering processes, involving the emission of a plasmon, can also be considered. There might also be interband scattering even though it is not clear how the momentum conservation in the circumferential direction would always be satisfied, because the momentum along the circumferential direction for the plasmon is not considered explicitly in this model. If there is scattering to the linear energy bands by the electron-plasmon interaction, this gives the following additional contribution to Eq. (6):

$$\frac{8E_g}{\pi \hbar^3 v_F} \frac{g_{\text{pl}}}{(1 + 1/g_{\text{pl}})} |V_{\text{el-pl}}|^2. \tag{7}$$

Here $E_g$ is the energy gap between the crosspoint of the two linear energy bands and the bottom of the band $c_1$, and this energy difference is about 1 eV. Using the value of $v_F = 8 \times 10^5$ m/s, we get $\gamma \simeq 0.4$ eV. We note that these estima-

tions also depend on the TL interaction parameter $g_{pl}$ as shown in Eqs. (6) and (7). The value of $g_{pl}$ would be close to 0.2 for the isolated condition, and then the $\gamma$ value would be 10 times smaller than the above estimations, which then become the same order of magnitude as the observed $\gamma_{EX}$ value.

Even though the discussion given above is still in the form of a qualitative estimation, we think that the electron-plasmon interaction plays an important role in the relaxation processes for *M*-SWNTs.

## IV. SUMMARY

In this paper, we have discussed how to calculate the resonance window of Raman spectra in SWNTs, and we have compared the results of the calculations with experiment. We calculated the $\gamma$ value as the lifetime of an excited electron, starting from identifying the resonance width with the energy dissipation, i.e., the lifetime of the carriers. For the result, in the case of *S*-SWNTs, we can get calculated $\gamma$ values in agreement with experiment, by just considering the electron-phonon coupling model. We can see that the $\gamma$ value shows a strong dependence on chirality and diameter for *S*-SWNTs. However, the $\gamma$ value calculation for *M*-SWNTs needs an additional contribution, such as might come from the electron-plasmon interaction, because the calculated $\gamma$ value that considers only the electron-phonon interaction is not consistent with experimental results, i.e., we get a considerably underestimated $\gamma$ value compared with experiment. The interaction between the excited electron in the conduction band and the plasmon on two linear energy bands gives almost the same order of magnitude for $\gamma$ as the $\gamma_{EX}$ value despite using very rough numerical estimations. In order to apply a detailed electron-plasmon effect to the $\gamma$ value calculation, further work is needed.

*Corresponding author. FAX: +81-22-795-6447; Electronic address: park@flex.phys.tohoku.ac.jp

†Electronic address: rsaito@flex.phys.tohoku.ac.jp

[1] M. S. Dresselhaus, G. Dresselhaus, R. Saito, and A. Jorio, Phys. Rep. **409**, 47 (2005).

[2] A. Jorio, A. P. Santos, H. B. Ribeiro, C. Fantini, M. Souza, J. P. M. Vieira, C. A. Furtado, J. Jiang, R. Saito, L. Balzano, D. E. Resasco, and M. A. Pimenta, Phys. Rev. B **72**, 075207 (2005).

[3] Ge. G. Samsonidze, R. Saito, N. Kobayashi, A. Grüneis, J. Jiang, A. Jorio, S. G. Chou, G. Dresselhaus, and M. S. Dresselhaus, Appl. Phys. Lett. **85**, 5703 (2004).

[4] J. Jiang, R. Saito, Ge. G. Samsonidze, S. G. Chou, A. Jorio, G. Dresselhaus, and M. S. Dresselhaus, Phys. Rev. B **72**, 235408 (2005).

[5] J. Jiang, R. Saito, A. Grüneis, S. G. Chou, Ge. G. Samsonidze, A. Jorio, G. Dresselhaus, and M. S. Dresselhaus, Phys. Rev. B **71**, 205420 (2005).

[6] Y. Oyama, R. Saito, K. Sato, J. Jiang, Ge. G. Samsonidze, A. Grüneis, Y. Miyauchi, S. Maruyama, A. Jorio, G. Dresselhaus, and M. S. Dresselhaus, Carbon **44**, 873 (2006).

[7] A. Jorio, C. Fantini, M. A. Pimenta, D. A. Heller, M. S. Strano, M. S. Dresselhaus, Y. Oyama, J. Jiang, and R. Saito, Appl. Phys. Lett. **88**, 023109 (2006).

[8] T. Okazaki, T. Saito, K. Matsuura, S. Ohshima, M. Yumura, Y. Oyama, R. Saito, and S. Iijima, Chem. Phys. Lett. **420**, 286 (2005).

[9] C. Fantini, A. Jorio, M. Souza, M. S. Strano, M. S. Dresselhaus, and M. A. Pimenta, Phys. Rev. Lett. **93**, 147406 (2004).

[10] J. Jiang, R. Saito, A. Grüneis, G. Dresselhaus, and M. S. Dresselhaus, Chem. Phys. Lett. **392**, 383 (2004).

[11] N. Akima, Y. Iwasa, S. Brown, A. M. Barbour, J. Cao, J. L. Musfeldt, H. Matsui, N. Toyota, M. Shiraishi, H. Shimoda, and O. Zhou, Adv. Mater. (Weinheim, Ger.) **18**, 1166 (2006).

[12] B. Kitiyanan, W. E. Alvarez, J. H. Harwell, and D. E. Resasco, Chem. Phys. Lett. **317**, 497 (2000).

[13] P. Nikolaev, M. J. Bronikowski, R. K. Bradley, F. Rohmund, D. T. Colbert, K. A. Smith, and R. E. Smalley, Chem. Phys. Lett. **313**, 91 (1999).

[14] J. Jiang, R. Saito, A. Grüneis, S. G. Chou, Ge. G. Samsonidze, A. Jorio, G. Dresselhaus, and M. S. Dresselhaus, Phys. Rev. B **71**, 045417 (2005).

[15] C. F. Klingshirn, *Semiconductor Optics* (Springer, Berlin, 2004).

[16] R. Saito, G. Dresselhaus, and M. S. Dresselhaus, Phys. Rev. B **61**, 2981 (2000).

[17] R. Egger and A. O. Gogolin, Phys. Rev. Lett. **79**, 5082 (1997).

[18] C. Kane, L. Balents, and M. P. A. Fisher, Phys. Rev. Lett. **79**, 5086 (1997).

[19] R. Egger and A. O. Gogolin, Eur. Phys. J. B **3**, 281 (1998).

[20] W. Izumida and M. Grifoni, New J. Phys. **7**, 244 (2005).

[21] T. Hertel and G. Moos, Chem. Phys. Lett. **320**, 359 (2000).

[22] T. Hertel and G. Moos, Phys. Rev. Lett. **84**, 5002 (2000).